Title
A satellite-based global landslide model

Author
Farahmand, Alireza

Publication Date
2013-04-01

Peer reviewed

UNIVERSITY OF CALIFORNIA,
IRVINE

A satellite-based global landslide model

Thesis

Submitted in partial satisfaction of the requirements
of the degree

MASTER OF SCIENCE

in Civil Engineering

by

Alireza Farahmand

Thesis Committee:

Professor Amir AghaKouchak, Chair
Professor Soroosh Sorooshian
Professor Kristen Davis

2013

TABLE OF CONTENTS

LIST OF FIGURES

LIST OF TABLES

Page

ACKNOWLEDGMENTS

I would like to express my deepest appreciation for my committee chair, Professor Amir AghaKouchak who has helped me in the preparation of this thesis. Without his guidance, this thesis would not be possible.

I would like to thank my committee members Professor Soroosh Sorooshian and Professor Kristen Davis for their efforts on reviewing this dissertation.

Also, I thank Natural Hazards and Earth System Science (NHESS) journal for their permission in sharing the copyrighted material of my paper.

Financial support was provided from the Academic Senate Council on Research, Computing, and Libraries (CORCL).

The text of this thesis/dissertation is a reprint of the material as it appears in "Farahmand, A., AghaKouchak, A., A satellite-based global landslide model, NHESS, 13: 1259–1267, 2013". The co-author listed in this publication, Professor Amir AghaKouchak directed and supervised research which forms the basis for the thesis/dissertation.

A satellite-based global landslide model

By

Alireza Farahmand

Master of Science in Civil and Environmental Engineering

University of California, Irvine, 2013

Professor Amir AghaKouchak, Chair

Landslides are devastating phenomena that cause huge damages around the world. This paper presents a quasi-global landslide model derived using satellite precipitation data, land-use land cover maps, and 250 m topography information. This suggested landslide model is based on the Support Vector Machines (SVM), a machine learning algorithm. The National Aeronautics and Space Administration (NASA) Goddard Space Flight Center (GSFC) land-slide inventory data is used as observations and reference data. 70% of the data are used for model development and training, whereas 30% are used for validation and verification. The results of 100 random sub-samples of available landslide observations revealed that the suggested landslide model can predict historical landslides reliably. The average error of 100 iterations of landslide prediction is estimated approximately 7%, while approximately 2% false landslide events are observed.

Chapter 1

Introduction

Each year, landslides cause thousands of casualties and billions of dollars in damages across the world. According to the US Geological Survey (USGS), landslides result in 10 of deaths and over 1-2 billion in property damages ([47]). For example, the Western United States has suffered from several storm-triggered landslides during the El Nino seasons of 1982-1983, resulting in millions of dollars in loss ([20]; [44]). In several other landslide events, thousands of people died or disappeared within a few minutes/hours (e.g., 1999 landslide in Vargas, Venezuela; see [32]).Also, in Southeast Asia, landslides are one of the most widespread disasters mainly because of the climate condition, mountainous terrain and socioeconomic conditions ([3]). For instance, in 2006, after a period of heavy rainfall, a series of landslides in the Leyte Island, Philippines claimed over 1000 fatalities ([39]).

The factors involved in the occurrence of landslides are divided into two categories: triggering processes and preparatory conditions ([13]). Triggering factors are dynamic processes which trigger a slope failure, such as heavy precipitation events (e.g., 1999 landslide in Vargas, Venezuela) and/or earthquakes (e.g., 2008 Wenchuan earthquake in Sichuan, China). Typically, hurricanes and typhoons lead to extensive rainfall over several days and thus,

may trigger landslides. In 1998, Hurricane Mitch alone triggered over 9,800 landslides across Guatemala resulting in over 14,000 casualties ([7]).

In addition to the presence of a triggering factor, preparatory conditions play important roles in the occurrence of landslides. These include conditions which make a region susceptible to landslides such as soil property, slope, topography, land use land cover, hillslope saturation and vegetation. For example, the effect of pore water pressure and soil porosity on the occurrence of landslides has been discussed in [25].

Thus far, various statistical, analytical and numerical approaches have been introduced to model landslides ([11]; [10], [45], [14], [38]; [6]; [48]; [40]; [26]; [41]; [46]; [50]; [9]; [31]). Based on the soil wetness condition and topographic attributes, [36] has offered a simplified Geographic Information System (GIS) based Bayesian model to identify landslides. Using satellite data and GIS techniques, [22] proposed a methodology to map landslide susceptibility. The approach is based on a weighted linear combination of landslide controlling factors including slope, soil type and texture, elevation, land cover type, and drainage density.

Rainfall intensity duration curves both in regional ([33]; [16]) and global scales ([8]; [20]; [21]) have been used in developing landslide models. The model presented in [8] is based on a rain gauge precipitation observations, while [8] is based on Tropical Rainfall Measurement Mission (TRMM) Multi-satellite Precipitation Analysis (TMPA; [24]).

In a recent effort, the National Aeronautics and Space Administration (NASA) Goddard Space Flight Center (GSFC) released a valuable inventory of landslide events over the globe ([29]). It can potentially be used for more detailed research on the relationship between landslide events, controlling factors and climate conditions. The NASA global landslide inventory has been evaluated in a number of landslide studies (e.g., [30]; [20]).

Most previous landslide studies have been in a local or regional scale (e.g., ([45]; [48]; [28]; [35]; [46]; [11]; [50]; [17]; [9]; [36]; [18]; [34]). This study introduces a quasi-global (hereafter,

global) landslide monitoring model using satellite precipitation data, land-use land cover maps, and 250 m topography information. This suggested landslide model is based on the Support Vector Machines (SVM) that can classify landslide and non-landslide events based on their climatological and geographical conditions.

Chapter 2

Study Area and Data Resources

The study area extends from -60 to +60 latitudes where real-time satellite precipitation data is available. The data sets used in this study include:

- NASA global landslide inventory ([29]): This data set represents landslides, mudslides, rockslides, debris slides and a combination of two or more of them. It includes nominal location information (country, county, city), time of occurrence, triggering factor, type of the event, relative size of landslide, geographic location (latitude and longitude) with a measure of location accuracy and impact information such as casualties and economic damage. The relative size classification is based on a scale of 1 (small landslide or mudslide) to 5 (massive landslide). The location accuracy classification is defined based on the radius of confidence on a scale of 1 (>75 km - little confidence in landslide location) to 5 (<5 km - high confidence in landslide location). Currently, the landslide inventory includes events occurred in 2003, 2007, 2008 and 2009. For more information about this landslide inventory, please refer to [29].

- Precipitation data: Satellite precipitation data is obtained from the real-time version of the Precipitation Estimation from Remotely Sensed Information Using Artificial

Neural Networks (PERSIANN; [23]; [43]). This data set is primarily based on longwave infrared imagery from geosynchronous satellite (GOES-IR) calibrated with satellite microwave data.

- Slope: Topographical information is derived based on a Digital Elevation Model (DEM) from the NASA Shuttle Radar Topography Mission ([27]). This data set is a high resolution elevation information with a spatial resolution of 250 m. Based on this elevation data set, a global slope map is created using Geographical Information System (GIS) techniques.

- Global land cover condition: Land-use land cover information is derived from a global database described in [4] and [15]. This data set includes 1 km land use land cover information with 23 classes.

Chapter 3

Methodology

The model concept is based on the SVM which is a powerful method for classification. In fact, SVM is a decision support machine that can be used to as a two-class or multiple class classifier. In this study, SVM is used to classify landslide and non-landslide events based on historical observations (here, observed landslide events). SVM classification solves a convex optimization problem in which all local solutions (e.g., individual landslide events) are classified into a global optimum ([5]). Throughout this study, a conventional approach of splitting data into a 70% training and a 30% validation is used.

In this study, the linear classifier of SVM is used for classification of landslide from non-landslide events. Let the training set be $\{(\mathbf{x_i}, y_i)\}_{i=1,\ldots,n}$ where $\mathbf{x_i} \in R^N$, and $y_i \in \{-1, 1\}$ ([19]). $\mathbf{x_i}$ Represents the N dimensional patterns (here, 5 dimensions including three vectors of precipitation, topographical information and land use) and y_i is the class label (i.e., 1 for landslide and -1 for non-landslide events). Figure 3.1 schematically presents the SVM model concept for classification. In the figure, blue points correspond to the landslide label, whereas the red points refer to the non-landslide label. The green line in Figure 3.1 is the optimal hyperplane classifier, which connects the two convex hulls of two classes (i.e.,

landslide and non-landslide events) and has the same distance from each of the convex hulls.

The general form of the optimal SVM classifier (the green line in Figure 3.1) is $(\mathbf{w}.\mathbf{x})+b=0$, $\mathbf{w} \in R^N$ and $b \in R$, with the decision function for classification being ([19]):

$$f(x) = sign((\mathbf{w}.\mathbf{x}) + b) \tag{3.1}$$

There exists a $\mathbf{w}$ (vector) and a b (scalar) such that for all training sets ([12]):

$$\begin{cases} ((\mathbf{w}.\mathbf{x_i}) + b) \geq +1 & \text{if } y_i = 1 \\ \\ ((\mathbf{w}.\mathbf{x_i}) + b) \leq -1 & \text{if } y_i = -1 \end{cases} \tag{3.2}$$

The above inequalities can be written in the form ([12]):

$$y_i \times ((\mathbf{w}.\mathbf{x_i}) + b) > 1, i = 1, \ldots, n \tag{3.3}$$

Using the above inequality, one can show (see [12] for details and proof):

$$\begin{cases} min\frac{\mathbf{w}.\mathbf{x}}{|\mathbf{w}|} = \frac{1}{|\mathbf{w}|} & \text{for } y = 1 \\ \\ max\frac{\mathbf{w}.\mathbf{x}}{|\mathbf{w}|} = \frac{-1}{|\mathbf{w}|} & \text{for } y = -1 \end{cases} \tag{3.4}$$

where $|\mathbf{w}|$ is defined as $\sqrt{\mathbf{w}.\mathbf{w}}$. The distance between two convex hulls of the two classes is termed as ρ (see Figure 3.1) and can be expressed as:

$$\begin{aligned} \rho(\mathbf{w}, b) &= min\left(\frac{\mathbf{w}.\mathbf{x}}{|\mathbf{w}|}\right)_{y=1} - max\left(\frac{\mathbf{w}.\mathbf{x}}{|\mathbf{w}|}\right)_{y=-1} \\ &= \frac{1}{|\mathbf{w}|} - \frac{-1}{|\mathbf{w}|} \\ &= \frac{2}{|\mathbf{w}|} \end{aligned} \tag{3.5}$$

The optimal classifier can be obtained by maximizing the distance $\rho(\mathbf{w}, b)$. Let's denote the optimal SVM classifier as $(\mathbf{w_0}.\mathbf{x}) + b_0 = 0$ and hence, $\rho(\mathbf{w_0}, b_0) = 2/|\mathbf{w_0}|$. In other words, for classifying the two landslide and non-landslide labels, one needs to solve the optimization problem of maximizing the margin $\rho(\mathbf{w_0}, b_0)$. To maximize $\rho(\mathbf{w_0}, b_0)$, the term $|\mathbf{w_0}|$ should be minimized under the constraint $y_i \times ((\mathbf{w}.\mathbf{x_i}) + b) > 1$, $i = 1, \ldots, n$. This is a quadratic optimization problem that can be solved using the sequential minimal optimization(SMO) outlined in [37].

Figure 3.2 schematically describes the model structure. As shown, the input data include two types of static information (land use land cover condition and topographical information) and one dynamic input (precipitation). It should be noted that the coordinates of the observed landslide locations in the NASA landslide inventory are in fact approximate locations of landslides ([29]). Therefore, using the slopes of landslide coordinates could lead to misleading results. For this reason, instead of using the slope of the provided coordinates in the inventory, a Topography Index is used that indicates the 95th percentile of 250 m slope values in a 0.25^o box. Note that the 0.25^o is the original resolution of precipitation

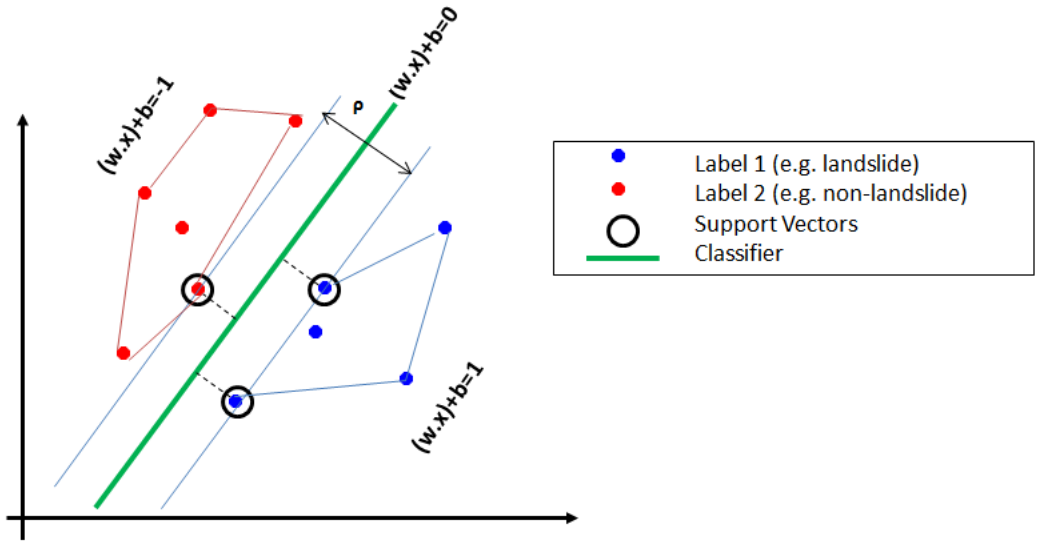

Figure 3.1: Support Vector Machine (SVM) model concept for classification.

Location #	Latitude	Longitude	Slope	Topography Index
1	34.972	54.983	0.09	0.14
2	-4.4032	136.0438	0.30	22.60

Table 3.1: Topography Index for two areas: The Lut Desert (location 1), which is flat and not susceptible to landslides; and a mountainous region in Indonesia (location 2), which has frequently experienced landslides

data. In other words, a Topography Index is used to distinguish topographically complex regions from relatively flat areas.

The suggested Topography Index is relatively larger for mountainous regions compared to flat areas. As an example, Table 3.1 lists the Topography Index for two areas: The Lut Desert (location 1 in Table 3.1), which is flat and not susceptible to landslides; and a mountainous region in Indonesia (location 2 in Table 3.1), which has previously experienced landslides. One can see that the slopes of the two locations are not significantly different (location 1: 0.09; location 2: 0.30 - see column 4 in Table 3.1). However, the Topography Index distinguishes the difference between the two regions (location 1 (flat region): 0.14; location 2 (mountainous region): 22.6 - see column 5 in Table 3.1).

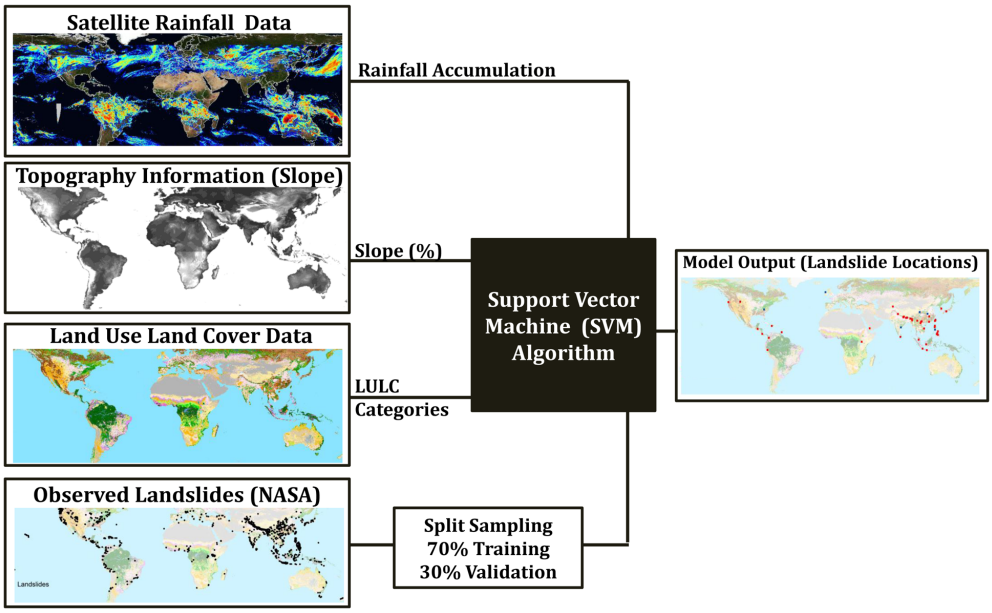

Figure 3.2: Schematic view of the model structure.

In addition to topography index, precipitation is used as a dynamic input in the model. There are two key factors associated with a rainfall that could lead to a landslide: intensity and duration. Landslides may occur due to heavy precipitation rates in a relatively short period of time or even after a low intensity rainfall over a long period of time. For this reason, three vectors of precipitation rates from rainfall accumulations in the past are used as input to the model: (a) 24 hr; (b) 48 hr; and (c) 72 hr. In a recent study, [2] showed that there are high uncertainties associated to satellite-based heavy precipitation rates at high temporal intervals (e.g., 3 hr - see also [1]). For this reason, at any given time, rainfall accumulations over the past 24, 48, and 72 hours are used as input to the model.

The soil wetness condition is indirectly computed from the past three-day rainfall information. Figure 3.3 displays the 24-hr precipitation accumulation (on the day of landslide occurrence) for the entire observed landslide events used in the model for both training and validation. One can see that the observations include 581 landslide events with 24-hr rainfall accumulations from 5 mm to over 200 mm. Note that the original NASA landslide inventory

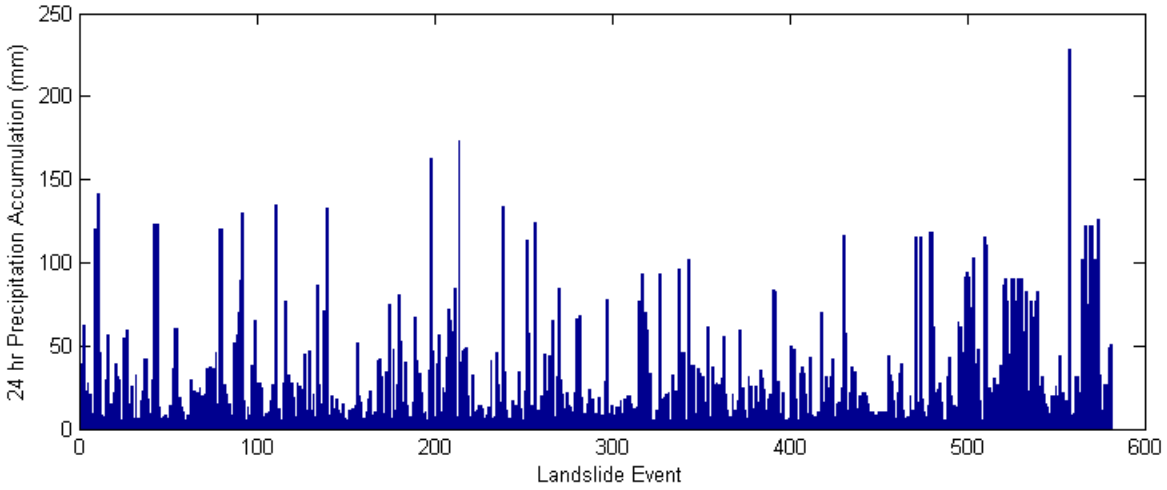

Figure 3.3: 24-hr precipitation accumulations over landslide observation points.

includes more landslide events. However, many of the events may not have been triggered by rainfall, as no rainfall has been recorded (earthquake triggered landslides). Alternatively, satellite data may have missed precipitation for a number of landslide events. Since the presented model is solely designed for rainfall triggered landslide events, those with 24-hr rainfall accumulation of 5 mm or less were eliminated from the analysis.

It should be noted that few landslide events are recorded in the landslide inventory with slopes and Topography Index near zero (below 10%), and these were also eliminated. In other words, the presented mode is designed and validated for rainfall triggered landslides for areas with a Topography Index $> 10\%$. Figure 3.4 displays the histogram of the Topography Index for the 581 landslides events that are used as input to the model. The horizontal axis shows Topography Index intervals, while the vertical axis displays the number of landslides in each interval.

As mentioned earlier, land-use land cover information is used as a static input to the model. Figure 3.5 shows the histogram of the observed landslides. The horizontal axis represents the 23 land use land cover categories listed in Table 3.2, whereas the vertical axis indicates

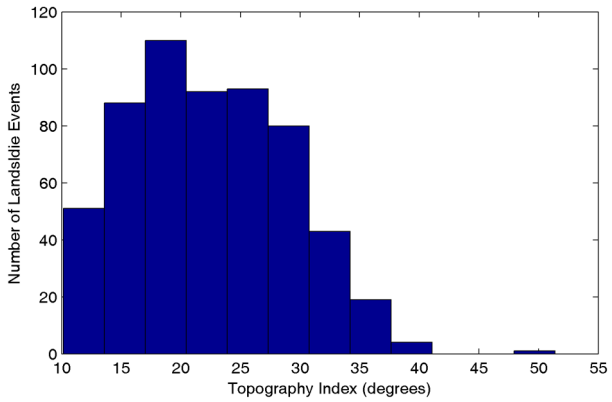

Figure 3.4: Histogram of Topography Index for landslide observations based on 250m Digital Elevation Model (DEM)

the number of occurrences in each land use land cover category. The observed landslides are then re-categorized into four major groups based on their land use land cover conditions: Tree Cover (# categories 1 to 10); Shrub Cover (#categories 11 to 15); Artificial Surfaces (categories 16 to 18 and 22); and Bare Areas (# 19). Note that Water Bodies, Snow and Ice and No Data (# 20, 21, 23) are eliminated from the analysis. This re-categorization is based on similarities between land-use land cover conditions. Finally, the distribution of landslide occurrences in the recategorized land use land cover conditions is presented in Figure 3.6. Based on the recategorized data, Artificial Surfaces (46%) and Tree Cover (38%) are more susceptible to landslides as more events have occurred in the past. The four re-categorized groups are scaled between 0 and 1 (Artificial Surfaces) with one being the most susceptible land use to landslides.

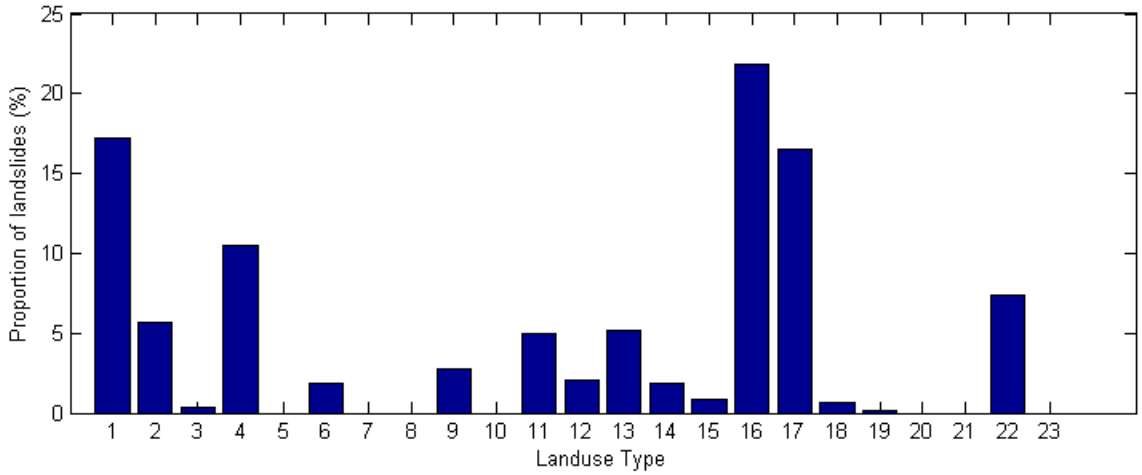

Figure 3.5: Distribution of landslides in the 23 land use land cover classes listed in Table 3.2

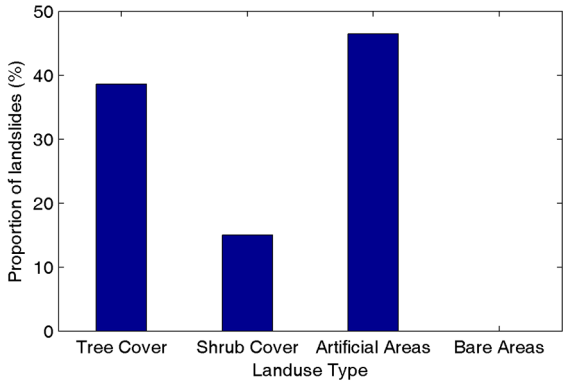

Figure 3.6: Distribution of landslides in the four re-categorized land cover classes

Table 3.2: The land use land cover classes in [4] and [15]

Number	Land Use Type
1	Tree Cover, Broadleaved, Evergreen
2	Tree Cover, Broadleaved, Deciduous, Closed
3	Tree Cover, Broadleaved, Deciduous, Open
4	Tree Cover, Needleleaved, Evergreen
5	Tree Cover, Needleleaved, Deciduous
6	Tree Cover, Mixed leaf type
7	Tree Cover, Regularly Flooded, Fresh Water
8	Tree Cover, Regularly Flooded, Saline Water
9	Mosaic, Tree Cover, Other Natural Vegetation
10	Tree Cover, Burnt
11	Shrub cover, Closed-Open, Evergreen
12	Shrub cover, closed-Open, Deciduous
13	Herbaceous Cover, Closed-Open
14	Sparse Herbaceous or Sparse Shrub Cover
15	Regularly Flooded Shrub and/or Herbaceous Cover
16	Cultivated and Managed Areas
17	Mosaic, Cropland, Tree Cover, Other Natural Vegetation
18	Mosaic, cropland, Shrub Cover or Grass Cover
19	Bare Areas
20	Water Bodies
21	Snow and Ice
22	Artificial Surfaces and Associate Areas
23	No Data

Chapter 4

Results and Discussion

The SVM is a machine learning algorithm that requires data from training and validation. In this study, 70% of the 581 landslide observations are used for model training and 30% for model validation and verification. The model builds a classifier, called the SVM classifier, based on the training data. The SVM classifier is then be validated using the validation data set. The target of the SVM classifier is either 0 or 1 . Zero represents a non-landslide condition, while one indicates the occurrence of a landslide event. If both model output and target lead to the same value (either 0 or 1), the algorithm has successfully classified landslides from non-landslide events. Otherwise, the model has failed to predict the event. Model output of 1 with a target of 0 indicates a false landslide prediction. On the other hand, a model output of 0 with a target of 1 indicates missed landslide prediction.

In the following example, a total of 6,391 events (581 landslide events and 5,810 non-landslide events) are sampled from across the globe. The 5,810 non-landslide events are sampled from precipitation areas and from different land use land cover conditions and slopes from all over the world. Samples are randomly taken from 2003, 2007, 2008 and 2009 for which observations are available. Of course the target values of non-landslide events are set to 0

and observed events are set to 1.

In order to ensure stability of the results, the 70 percent training data was randomly sampled 100 times. In other words, the results are tested by running the model 100 times with different combinations of training and validation data. Figure 4.1(a) presents the overall error of the model landslide prediction in percentage. In Figure 4.1(a), the horizontal axis represents the iterations (i.e., 100), and the vertical axis displays the error (%) that includes the error of both landslide and non-landslide events. As shown, the average error is between 6 to 7 percent in 100 iterations. In order to provide more insight, two other error plots are presented: missed landslides (Figure 4.1(b)) and false landslides (Figure 4.1(c)). Here, false and missed events are calculated based on the common approach used for validation of remote sensing data as outlined in [49]. The missed landslide plot (Figure 4.1(b)) indicates the error in the number of missed landslide events divided by the total number of landslide observations used for validation. On the other hand, 4.1(c) displays the error in the number of falsely predicted events divided by the total number of non-landslide samples. Note that this model does not attempt to simulate landslides where the slope is less than 10 degree and 24-hr precipitation accumulation is less than 5mm (same conditions applied to sample from landslide observations). One can see that the missed and false landslide errors are approximately 7 and 2 percent, respectively (see Figures 4.1(b) and (c)).

Figure 4.1(b) indicates that the error of missed landslides at few iterations is very high. This is due to limited number of observed landslides that could lead in no or limited sample from certain types of landslides for training. For this reason, one needs to run the model with multiple randomly selected samples of training and validation to make sure the training data is sufficient for landslide modeling and prediction. In this example, one can see that many combinations of training and validation lead to a small error in missed landslides.

For better illustration, Figure 4.2 displays the SVM-based model output for one iteration. In Figure 4.2, red circles indicate landslides identified correctly, whereas blue circles show non-

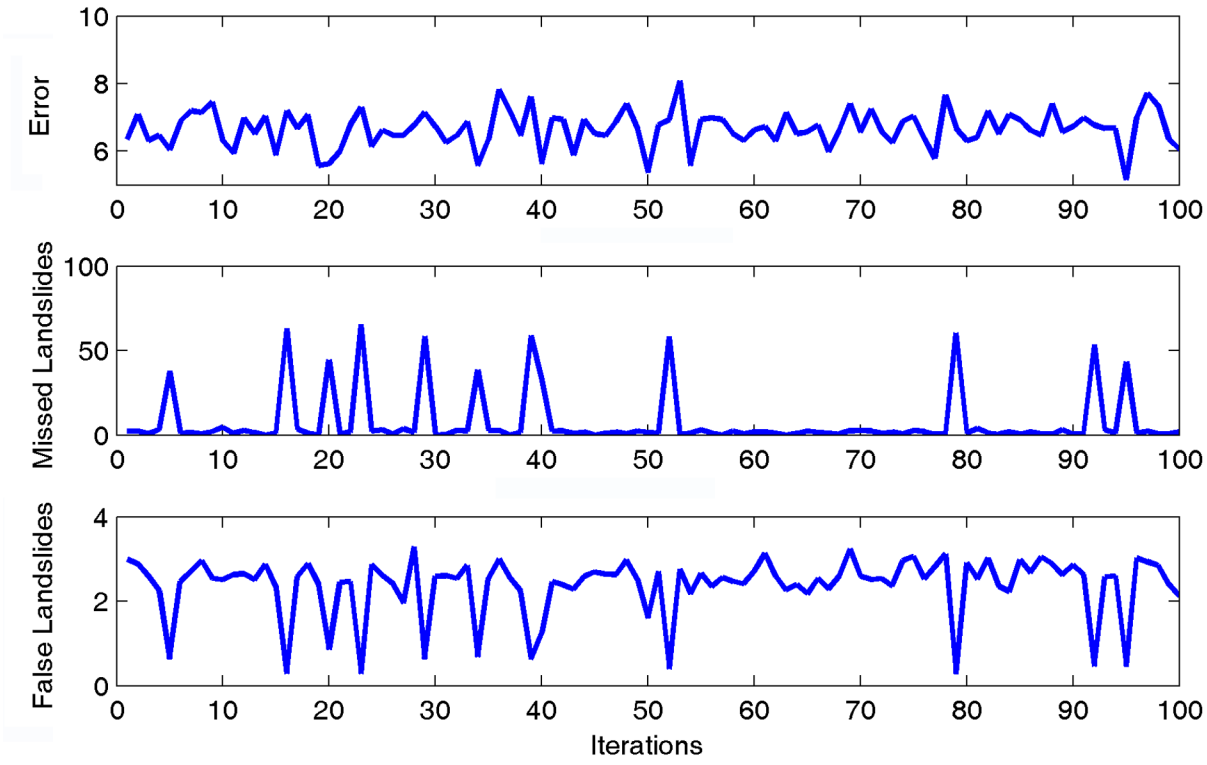

Figure 4.1: (a) Total error; (b) Error of missed landslides; and (c) Error of false landslides of the model for 100 simulations with different combinations of 70% training and 30% validation data

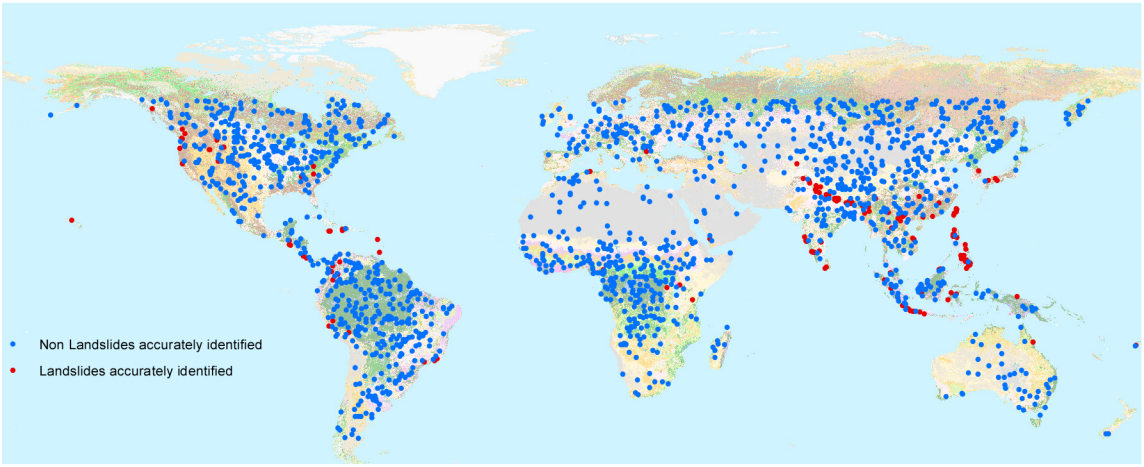

Figure 4.2: An example of the SVM-based model output for one iteration. The red circles indicate landslides identified correctly, whereas blue circles show non-landslides identified correctly

landslides identified correctly. For the same iteration, Figure 4.3 displays false landslides (red squares) and missed landslides (blue squares) - events incorrectly identified by the model. In other words, in figure 4.3, the red squares are non-landslide events detected incorrectly as landslides by the model. Similarly, blue squares are actual landslide events that the model failed to detect.

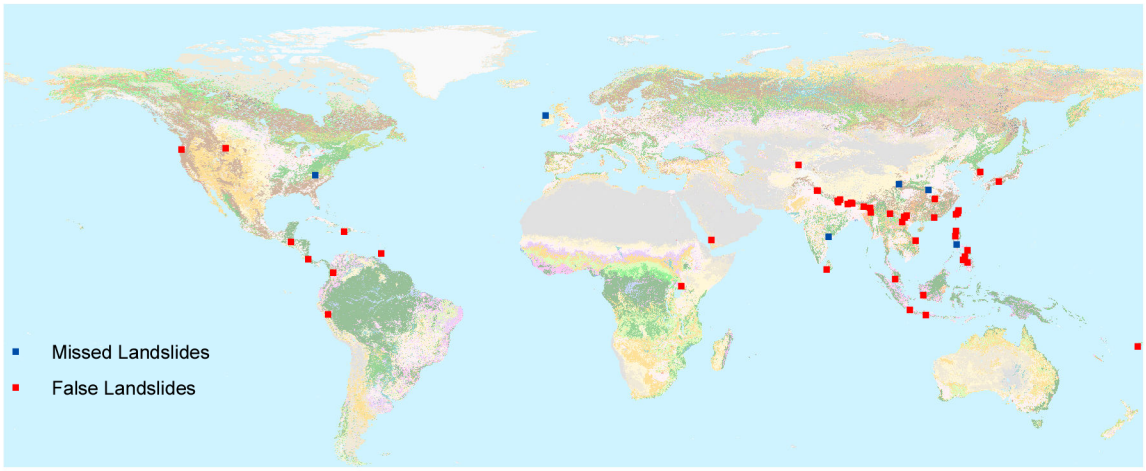

Figure 4.3: False landslides (red squares) and missed landslides (blue squares) for the same iteration shown in Figure 4.2.

Chapter 5

conclusions

Landslides are devastating phenomena that cause huge damages around the world. This paper presents a quasi-global landslide model using SVM approach. The input data include satellite precipitation data, land-use land cover maps, and 250 m topography information. The model was tested and verified against the NASA GSFC landslide inventory data. Throughout the study, 70% of the data were used for model development and training, while 30% were used for validation and verification.

The model was used to simulate 100 iterations with random sub-samples of 70% training and 30% validation. It should be noted that a large number of non-landslide events (10 times more than the observations) were randomly sampled to evaluate the performance of the model in detecting both landslides and non-landslide events. The results showed that the suggested landslide model can predict historical landslides reliably. The average error of 100 iterations of landslide prediction was estimated as approximately 6 to 7%, while approximately 2% false landslide and approximately 7% missed landslide events were observed.

The authors point out that these conclusions are based on exploratory data analysis using observed records of landslide events. We acknowledge that remotely sensed precipitation

events have uncertainties, especially with respect to heavy precipitation rates ([1]) that could affect landslide monitoring and prediction. However, satellite data sets are the only source of real-time and consistent precipitation observations especially over remote and topographically complex regions ([42]). In fact, landslides typically occur in mountainous regions where other sources of information (e.g., radar and gauge measurements) are not available. For this reason, the model has been developed with satellite observation so that it can be applied to remote and topographically complex regions. This model cannot be considered as a general landslide model as it does not consider earthquake triggered landslides. Efforts are underway to further develop this model into a real-time landslide prediction model.

Bibliography

[1] A. AghaKouchak, A. Behrangi, S. Sorooshian, K. Hsu, and E. Amitai. Evaluation of satellite-retrieved extreme precipitation rates across the central United States. *Journal of Geophysical Research-Atmospheres*, 116, 2011.

[2] A. AghaKouchak, A. Mehran, H. Norouzi, and A. Behrangi. Systematic and random error components in satellite precipitation data sets. *Geophysical Research Letters*, 39(9):L09406, 2012.

[3] Apip, K. Takara, Y. Yamashiki, K. Sassa, A. B. Ibrahim, and H. Fukuoka. A distributed hydrological-geotechnical model using satellite-derived rainfall estimates for shallow landslide prediction system at a catchment scale. *Landslides*, 7(3):237–258, 2010.

[4] Bartholome at al. *GLC 2000 Global Land Cover mapping for the year 2000*. European Commission, DG Joint Research Centre, Luxemburg, 2002.

[5] C. Bishop. Neural networks and their applications. *Review of Scientific Instruments*, 65(6):1803–1832, 1994.

[6] C. Bovolo and J. Bathurst. Modelling catchment-scale shallow landslide occurrence and sediment yield as a function of rainfall return period. *Hydrological Processes*, 2011. doi: 10.1002/hyp.8158.

[7] R. Bucknam, J. Coe, M. Chavarria, J. Godt, A. Tarr, L. Bradley, S. Rafferty, D. Hancock, R. Dart, and M. Johnson. Landslides triggered by hurricane mitch in guatemala - inventory and discussion. Technical report, United States Geological Survey Open File Report 01-0443, 2001.

[8] N. Caine. The rainfall intensity: duration control of shallow landslides and debris flows. *Geografiska Annaler. Series A. Physical Geography*, pages 23–27, 1980.

[9] N. Casagli, F. Catani, C. Del Ventisette, and G. Luzi. Monitoring, prediction, and early warning using ground-based radar interferometry. *Landslides*, 7(3):291–301, 2010.

[10] N. Casagli, S. Dapporto, M. Ibsen, V. Tofani, and P. Vannocci. Analysis of the landslide triggering mechanism during the storm of 20th-21st November 2000, in Northern Tuscany. *Landslides*, 3(1):13–21, MAR 2006.

[11] F. Catani, N. Casagli, L. Ermini, G. Righini, and G. Menduni. Landslide hazard and risk mapping at catchment scale 2005 Arno River basin. *Landslides*, 2(4):329–342, DEC 2005.

[12] C. Cortes and V. Vapnik. Support-vector networks. *Machine learning*, 20(3):273–297, 1995.

[13] F. Dai, C. Lee, and Y. Ngai. Landslide risk assessment and management: an overview. *Engineering geology*, 64(1):65–87, 2002.

[14] L. Ermini, F. Catani, and N. Casagli. Artificial Neural Networks applied to landslide susceptibility assessment. *Geomorphology*, 66(1-4):327–343, MAR 1 2005.

[15] S. Fritz, E. Bartholome, A. Belward, A. Hartley, J.-H. Stibig, H. Eva, P. Mayaux, S. Bartalev, R. Latifovic, S. Kolmert, and et al. Harmonisation, mosaicing and production of the global land cover 2000 database. Technical report, European Commission, DG Joint Research Centre, 2003.

[16] J. W. Godt, R. L. Baum, and A. F. Chleborad. Rainfall characteristics for shallow landsliding in seattle, washington, usa. *Earth Surface Processes and Landforms*, 31(1):97–110, 2006.

[17] A. Guenther and C. Thiel. Combined rock slope stability and shallow landslide susceptibility assessment of the Jasmund cliff area (Rugen Island, Germany). *Natural Hazards and Earth System Sciences*, 9(3):687–698, 2009.

[18] F. Guzzetti, P. Reichenbach, M. Cardinali, M. Galli, and F. Ardizzone. Probabilistic landslide hazard assessment at the basin scale. *Geomorphology*, 72(1):272–299, 2005.

[19] M. A. Hearst, S. Dumais, E. Osman, J. Platt, and B. Scholkopf. Support vector machines. *Intelligent Systems and their Applications, IEEE*, 13(4):18–28, 1998.

[20] Y. Hong, R. Adler, and G. Huffman. Evaluation of the potential of NASA multi-satellite precipitation analysis in global landslide hazard assessment. *Geophysical Research Letters*, 33(22), 2006.

[21] Y. Hong, R. Adler, and G. Huffman. Satellite remote sensing for global landslide monitoring. *Eos*, 88(37), 2007.

[22] Y. Hong, R. Adler, and G. Huffman. Use of satellite remote sensing data in the mapping of global landslide susceptibility. *Natural Hazards*, 43(2):245–256, 2007.

[23] K. Hsu, X. Gao, S. Sorooshian, and H. Gupta. Precipitation estimation from remotely sensed information using artificial neural networks. *Journal of Applied Meteorology*, 36:11761190, 1997.

[24] G. Huffman, R. Adler, D. Bolvin, G. Gu, E. Nelkin, K. Bowman, E. Stocker, and D. Wolff. The trmm multi-satellite precipitation analysis: Quasi-global, multiyear, combined-sensor precipitation estimates at fine scale. *J. Hydrometeorol.*, 8:3855, 2007.

[25] R. Iverson, M. Reid, N. Iverson, R. LaHusen, M. Logan, J. Mann, and D. Brien. Acute sensitivity of landslide rates to initial soil porosity. *Science*, 290(5491):513–516, 2000.

[26] M. Jaboyedoff, T. Oppikofer, A. Abellan, M.-H. Derron, A. Loye, R. Metzger, and A. Pedrazzini. Use of LIDAR in landslide investigations: a review. *Natural Hazards*, 61(1):5–28, MAR 2012.

[27] A. Jarvis, H. Reuter, A. Nelson, and E. Guevara. Hole-filled srtm for the globe version 4. Technical report, available from the CGIAR-CSI SRTM 90m Database, 2012.

[28] D. K. Keefer, R. C. Wilson, R. K. Mark, E. E. Brabb, W. Brown 3rd, S. D. Ellen, E. L. Harp, G. F. Wieczorek, C. S. Alger, and R. S. Zatkin. Real-time landslide warning during heavy rainfall. *Science (New York, NY)*, 238(4829):921, 1987.

[29] D. B. Kirschbaum, R. Adler, Y. Hong, S. Hill, and A. Lerner-Lam. A global landslide catalag for hazard applications: method, results, and limitations. *Springer*, 2009.

[30] D. B. Kirschbaum, R. Adler, Y. Hong, S. Hill, and A. Lerner-Lam. Evaluation of a preliminary satellite-based landslide hazard algorithm using global landslide inventories. *Springer*, 2009.

[31] D. B. Kirschbaum, R. Adler, Y. Hong, S. Kumar, C. Peters-Lidard, and A. Lerner-Lam. Advances in landslide nowcasting: evaluation of a global and regional modeling approach. *Environmental Earth Sciences*, pages 1–14, 2012.

[32] M. Larsen, G. Wieczorek, L. Eaton, H. Torres-Sierra, and B. Morgan. The december 1999 rainfall-triggered landslide and flash-flood disaster in vargas, venezuela. *Eos Transactions - AGU Fall Meet. Suppl.*, 81(48), 2000.

[33] M. C. Larsen and A. Simon. A rainfall intensity-duration threshold for landslides in a humid-tropical environment, puerto rico. *Geografiska Annaler. Series A. Physical Geography*, pages 13–23, 1993.

[34] C. Lepore, S. A. Kamal, P. Shanahan, and R. L. Bras. Rainfall-induced landslide susceptibility zonation of puerto rico. *Environmental Earth Sciences*, pages 1–15, 2012.

[35] Z. Liao, Y. Hong, D. Kirschbaum, and C. Liu. Assessment of shallow landslides from hurricane mitch in central america using a physically based model. *Environmental Earth Sciences*, pages 1–9, 2012.

[36] M. Lineback Gritzner, W. A. Marcus, R. Aspinall, and S. G. Custer. Assessing landslide potential using gis, soil wetness modeling and topographic attributes, payette river, idaho. *Geomorphology*, 37(1):149–165, 2001.

[37] J. C. Platt. 12 fast training of support vector machines using sequential minimal optimization. 1999.

[38] D. Ren, R. Fu, L. M. Leslie, and R. E. Dickinson. Predicting storm-triggered landslides. *Bulletin of the American Meteorological Society*, 92(2):129–139, 2011.

[39] K. Sassa, O. Nagai, R. Solidum, Y. Yamazaki, and H. Ohta. An integrated model simulating the initiation and motion of earthquake and rain induced rapid landslides and its application to the 2006 Leyte landslide. *Landslides*, 7(3):219–236, 2010.

[40] K. Sassa, S. Tsuchiya, K. Ugai, A. Wakai, and T. Uchimura. Landslides: a review of achievements in the first 5 years (2004-2009). *Landslides*, 6(4):275–286, 2009.

[41] S. Segoni, G. Rossi, and F. Catani. Improving basin scale shallow landslide modelling using reliable soil thickness maps. *Natural Hazards*, 61(1):85–101, MAR 2012.

[42] S. Sorooshian, A. AghaKouchak, P. Arkin, J. Eylander, E. Foufoula-Georgiou, R. Harmon, J. M. H. Hendrickx, B. Imam, R. Kuligowski, B. Skahill, and G. Skofronick-Jackson. Advanced concepts on remote sensing of precipitation at multiple scales. *Bulletin of the American Meteorological Society*, 92(10):1353–1357, 2011.

[43] S. Sorooshian, K. Hsu, X. Gao, H. Gupta, B. Imam, and D. Braithwaite. Evolution of the persiann system satellite-based estimates of tropical rainfall. *Bull. Am. Meteorol. Soc.*, 81(9):2035 2046, 2000.

[44] E. Spiker and P. Gori. National landslide hazards mitigation strategy - a framework for loss reduction. *U.S. Geological Survey Circulars*, 1244:1 64, 2003.

[45] V. Tofani, S. Dapporto, P. Vannocci, and N. Casagli. Infiltration, seepage and slope instability mechanisms during the 20-21 November 2000 rainstorm in Tuscany, central Italy. *Natural Hazards and Earth System Sciences*, 6(6):1025–1033, 2006.

[46] T. Uchimura, I. Towhata, T. T. L. Anh, J. Fukuda, C. J. B. Bautista, L. Wang, I. Seko, T. Uchida, A. Matsuoka, Y. Ito, Y. Onda, S. Iwagami, M.-S. Kim, and N. Sakai. Simple monitoring method for precaution of landslides watching tilting and water contents on slopes surface. *Landslides*, 7(3):351–357, 2010.

[47] USGS. landslide hazard program. Technical report, United States Geological Survey, 2006.

[48] G. F. Wieczorek and P. P. Leahy. Landslide hazard mitigation in North America. *Environmental & Engineering Geoscience*, 14(2):133–144, 2008.

[49] D. Wilks. *Statistical Methods in the Atmospheric Sciences*. Academic Press, Burlington, MA (2nd edition), 2006.

[50] Y. Yin, H. Wang, Y. Gao, and X. Li. Real-time monitoring and early warning of landslides at relocated Wushan Town, the Three Gorges Reservoir, China. *Landslides*, 7(3):339–349, 2010.